

One-Step Aeroacoustics Simulation Using Lattice Boltzmann Method

X. M. Li,* R. C. K. Leung,† and R. M. C. So‡

Hong Kong Polytechnic University, Hong Kong, People's Republic of China

The lattice Boltzmann method (LBM) is a numerical simplification of the Boltzmann equation of the kinetic theory of gases that describes fluid motions by tracking the evolution of the particle velocity distribution function based on linear streaming with nonlinear collision. If the Bhatnagar–Gross–Krook (BGK) collision model is invoked, the velocity distribution function in this mesoscopic description of nonlinear fluid motions is essentially linear. This intrinsic feature of LBM can be exploited for convenient parallel programming, which makes itself particularly attractive for one-step aeroacoustics simulations. It is shown that the compressible Navier–Stokes equations and the ideal gas equation of state can be correctly recovered by considering the translational and rotational degrees of freedom of diatomic gases in the internal energy and using a multiscale Chapman–Enskog expansion. Assuming two relaxation times in the BGK model allows the temperature dependence of the first coefficient of viscosity of diatomic gases to be replicated. The modified LBM model is solved using a two-dimensional 9-discretized and a two-dimensional 13-discretized velocity lattices. Three cases are selected to validate the one-step LBM aeroacoustics simulation. They are the one-dimensional acoustic pulse propagation, the circular acoustic pulse propagation, and the propagation of acoustic, vorticity, and entropy pulses in a uniform stream. The accuracy of the LBM is established by comparing with direct numerical simulation (DNS) results obtained by solving the governing equations using a finite difference scheme. The tests show that the proposed LBM and the DNS give identical results, thus suggesting that the LBM can be used to simulate aeroacoustics problems correctly.

Nomenclature

c_p, c_v	= specific heats at constant pressure and constant volume
c_0	= speed of sound
D	= spatial dimension
D_T, D_R	= translational and rotational degrees of freedom of particle motion
e	= internal energy
F_{ex}	= external body force
f	= particle velocity distribution function
f^{eq}	= Maxwellian–Boltzmann equilibrium distribution function
f^{neq}	= nonequilibrium particle distribution function
h	= enthalpy
J	= approximation for Q
k_B	= Boltzmann constant
l	= length
M	= Mach number
M_n	= molecular mass
n	= particle number density
Pr	= Prandtl number
p	= thermodynamic pressure
Q	= collision operator
R	= gas constant
Re	= Reynolds number
r_m	= particle separation
S_0	= Sutherland constant

T	= temperature
T_{ref}	= Sutherland law reference temperature
t	= time
u	= velocity vector
u, v	= velocity components along x and y directions
γ	= specific heat ratio, c_p/c_v
$\delta_{\alpha\beta}$	= Kronecker delta
ε	= Knudsen number
κ	= thermal conductivity
κ'	= thermal diffusivity
λ	= second coefficient of viscosity
μ	= first coefficient of viscosity
ν	= index of repulsion
ξ	= velocity vector of fluid particle
ρ	= density
σ_m	= effective particle diameter
$\sigma(\Omega)$	= collision cross section
$\tau, \tau_1, \tau_2, \tau_{eff}$	= relaxation times
$\tau_{\alpha\beta}$	= viscous stress tensor
Φ	= dissipation rate
ψ	= collision invariants
Ω	= spatial angle
ω	= collision frequency
$\ $	= modulus

Subscripts

i	= indices of discrete lattice
α, β	= indices
0	= reference variables
∞	= mean flow quantities

Superscripts

$-$	= average values
\wedge	= peak values

Received 7 February 2005; revision received 20 July 2005; accepted for publication 26 July 2005. Copyright © 2005 by R. C. K. Leung and R. M. C. So. Published by the American Institute of Aeronautics and Astronautics, Inc., with permission. Copies of this paper may be made for personal or internal use, on condition that the copier pay the \$10.00 per-copy fee to the Copyright Clearance Center, Inc., 222 Rosewood Drive, Danvers, MA 01923; include the code 0001-1452/06 \$10.00 in correspondence with the CCC.

*Ph.D. Student, Department of Mechanical Engineering, Hung Hom, Kowloon.

†Assistant Professor, Department of Mechanical Engineering, Hung Hom, Kowloon. Senior Member AIAA.

‡Chair Professor and Head, Department of Mechanical Engineering, Hung Hom, Kowloon. Fellow AIAA.

I. Introduction

NOISE reduction is an important part of engineering design in the transportation industries. Airplane, automobiles, and trains

all produce noise that disturbs passengers, operators, and the surrounding communities. Examples of current interest include airframe noise, cavity acoustics, jet screech, sonic boom, cabin noise, and noise generated by blade/vortex interactions. In particular, the need to meet more stringent community noise-level standards has resulted in recent attention given to the relatively new field of time-domain computational aeroacoustics (CAA), which focuses on the accurate prediction of aerodynamic sound generated by airframe components and propulsion systems, as well as on its propagation and far-field characteristics. Both aspects of the problem, that is, sound generation and propagation, are extremely demanding from a time-domain computation standpoint due to the large number of grid points and small time steps that are typically required. Therefore, if realistic aeroacoustics simulations are to become more feasible, higher-order accurate and optimized numerical schemes have to be sought to reduce the number of grid points required per wavelength while still ensuring tolerable levels of numerically induced dissipation and dispersion.

There are two major categories of CAA simulation methodology, namely, hybrid methods and one-step or direct simulations.^{1,2} In hybrid methods, unsteady computational fluid dynamics simulations, such as direct numerical simulation (DNS) or large eddy simulation, are used to replicate the space-time properties of the noise-generating flow. The solutions are then treated as equivalent noise sources with distributed strength and used as inputs for a second calculation of the noise propagation to the far field. The noise calculation is usually achieved by exploiting Lighthill's acoustic analogy,³ or its derivative (see Ref. 4), by solving the linearized Euler equation (see Ref. 5), or by acoustic/viscous decomposition techniques.^{6,7} Usually two different meshes are required due to the different length scales of the flow and sound fields. Consequently, hybrid methods are not able to handle any interaction of the flow with the noise it generates and are, therefore, only good for noise-generation prediction. One-step simulations attempt to resolve both the unsteady flow and the sound in just one calculation. The computational mesh required is not only able to cover the source and observer regions, but also capable of resolving the different length scales of the two regions. The calculated flow and sound fields are required to leave the computational domain smoothly, and there is no nonphysical disturbances created by the domain boundaries.⁸ This is commonly achieved by laying artificial absorbing buffer regions around the entire domain to eliminate the outgoing waves before they touch the boundaries. High computational cost is required to satisfy all of these requirements for accurate one-step simulations. Even then, one-step simulations are still preferred because they can provide the details of sound generating mechanisms, as well as flow-sound interactions in complex flows.

Recent reviews of computational aeroacoustics have been given by Tam¹ and Wells and Renaut,⁹ who discuss various numerical schemes that are currently used in CAA. These include, among others, the dispersion-relation-preserving scheme of Tam and Webb,¹⁰ the family of higher-order compact differencing schemes of Lele,¹¹ the method for minimization of group velocity errors due to Holberg,¹² and the essentially nonoscillatory scheme.¹³ The first three schemes are all centered nondissipative schemes, a property that is desirable for linear wave propagation. However, the inherent lack of numerical dissipation may result in spurious numerical oscillations and instability in practical applications involving general geometries, approximate boundary conditions, or nonlinear features. In the dispersion-relation-preserving approach, for instance, artificial selective damping has to be employed under these conditions.¹ Although quite robust, standard upwind and upwind-biased formulations may be undesirable for situations involving linear wave propagation due to their excessive dissipation. To overcome this difficulty, higher-order upwind or essentially nonoscillatory approaches were proposed.¹⁴ These spatial semidiscretizations are typically combined with high-order explicit time-integration methods such as the multistage Runge-Kutta procedure (see Ref. 15). In addition to the spatial and temporal discretizations, another critical aspect in CAA simulations is the accurate treatment of the physical and computational boundary conditions. Recent reviews of radiation,

outflow, and wall boundary treatments are provided by Colonius⁸ and Tam.¹⁶ In most of these formulations, a continuum model is used to derive the governing equations from the Navier-Stokes and energy equations.

The Boltzmann equation (BE) describes the evolution of the particle velocity distribution function based on the free streaming and collisions of particles.^{17,18} The macroscopic quantities of the fluid, such as density, momentum, internal energy, and energy flux, are defined via moments of the distribution function. These relations constitute the kinetic equations. There are three major differences between the Navier-Stokes equations and the BE. First, the BE is applicable even if the medium could not be considered as continuous, such as in simulating rarefied gas flows or multiphase and multicomponent flows. Second, the BE provides clear physical definitions for the equation of state of the fluid, the viscous stress, and the heat conduction from the molecular transport viewpoint. For the Navier-Stokes equations, these considerations could not be derived directly from the continuum model. In general, the perfect gas equation of state, the Stokes viscous hypothesis, and the Fourier heat conduction relation have to be introduced to solve the equations. Third, there is a large timescale disparity between these two kinds of equations. In most fluids of practical interest, the velocity distribution function has a timescale equal to that of the collision interval time of the particles, which is of the order of $10^{-8} \sim 10^{-9}$ s for most practical ranges of pressure and temperature.¹⁹ On the other hand, the macroscopic quantities in the Navier-Stokes equations, such as density, velocity, pressure, and temperature, are affected by the long timescale of the velocity distribution function, which is of the order of about 10^{-4} s. Consequently, the BE has a much smaller timescale than the Navier-Stokes equations. However, the BE is relatively simple compared to the Navier-Stokes equations. Therefore, the numerical code could exploit the intrinsic features of parallelism. This makes it especially useful to model problems with complicated boundary conditions and with multiphase interfaces.

The lattice Boltzmann method (LBM) is derived from the lattice gas automata.¹⁸ As a simplified version of the BE, the LBM is discrete in phase (or velocity) space. It was proposed as an alternative to the conventional computational fluid dynamics techniques^{20,21} more than a decade ago. A variety of LBM models have been proposed for different hydrodynamic systems, such as single component hydrodynamics, multiphase and multicomponent flows, particle suspensions in fluid, reaction-diffusion systems, and flow through porous media.²² In kinetic theory of gases, the evolution of a fluid is described by the solutions to the continuous BE. Development of LBM for single-phase compressible flow, such as air, has received particular attention because its solution recovers the macroscopic Navier-Stokes equations in the asymptotic limit of Knudsen number (see Refs. 23–26). When a fully discrete particle velocity model was used, where space and time were discretized on a square lattice, internal energy of the particles was fixed. Therefore, the LBM was only used to simulate isothermal flows and low Mach number flows in the incompressible limit.^{27,28}

There have been attempts to incorporate the effects of temperature variations in the LBM to simulate compressible flows and wave propagation. Sun²⁹ introduced a potential energy term into the expression of particle energy in the LBM on hexagonal lattice for shock wave simulations. The potential energy term was not dependent on temperature but arbitrarily prescribed to recover the correct local specific heat ratio of all fluid particles. Thus modified, the LBM has serious limitations. The numerical results compared rather favorably with analytical solutions. This was accomplished by setting the relaxation time to unity. However, under this assumption, the first coefficient of viscosity would vary linearly with temperature and Sutherland law could not be recovered correctly. Palmer and Rector³⁰ attempted to incorporate the temperature effect by separately modeling the internal energy as a scalar field using a second distribution in addition to the isothermal LBM calculation. The energy is then properly accounted for in the evaluation of the density and the momentum of the fluid particles. Good agreement was obtained in several thermal convection test cases but the applicability of their model to aeroacoustics simulations is questionable because

the equation of state is not explicitly recovered. Tsutahara et al.³¹ and Kang et al.³² attempted to include the particle rotational energy into a modified LBM by solving an additional distribution function that is the product of velocity distribution and a rotational energy term. This model assumed monoatomic gas particles and gave rise to a constant specific heat ratio of 1.67. They calculated shock reflection and Aeolian tone generated by a circular cylinder and obtained qualitative agreement with DNS results. However, this was at the expense of having to specify 21 discrete velocities on a hexagonal lattice.

This paper focuses on the development of a one-step aeroacoustics simulation scheme using the LBM for two-dimensional flows. If the aeroacoustics calculations were to be correct, the ideal gas equation of state and the temperature dependence of the first coefficient of viscosity of the gas have to be recovered properly. Therefore, it is important to show that the LBM could satisfy these requirements. Furthermore, the credibility of the one-step LBM simulation of aeroacoustics has to be established, either by comparing the calculations with theoretical solutions or with DNS results.

In the next section is given a brief description of the set of unsteady compressible Navier–Stokes equations and their solution using a DNS technique where the governing equations are solved using higher-order schemes for spatial differencing and for time marching. This is followed by a discussion of the continuous Boltzmann equation and the kinetic energy equations for different particle velocity orders. It is shown that the set of unsteady compressible Navier–Stokes equations for real diatomic gas could be fully recovered with the specific heat ratio given by $\gamma = 1.4$ after the Chapman–Enskog expansion has been assumed for the expansion of the distribution function in the BE and the internal energy expression has been properly modified. In Sec. IV, the recovery of the correct temperature dependence of the first coefficient of viscosity as described by the Sutherland law is achieved provided the relaxation time for the collision model has been suitably adjusted to include the effect of the weak repulsive potential. Two velocity lattice models, a two-dimensional 9-discrete-velocity lattice (D2Q9) and a two-dimensional 13-discrete-velocity lattice (D2Q13), are introduced together with a higher-order finite difference scheme in Sec. V. Validations of the LBM against some basic acoustic pulses where analytical solutions are available are given in Sec. VI. In addition, the LBM solutions are also compared with one-step DNS solutions of a number of aeroacoustics problems. All comparisons show that the proposed LBM could be used to carry out one-step aeroacoustics simulations with equal accuracy as the DNS.

II. One-Step DNS Aeroacoustics Simulation

A one-step aeroacoustics simulation means that the sound field generated from unsteady flows and its propagation are calculated without having to carry out the calculations of aerodynamics and acoustics fields separately. Because the flow and acoustics fields are calculated simultaneously in a single computation, further investigations of the aerodynamic sound-generation mechanisms could be easily carried out. In aeroacoustics analysis, the fluid is usually modeled as a continuum and its unsteady dynamics is essentially determined by the fundamental principles of the conservation of mass, momentum, and energy at each fluid point in the continuum. The acoustic fluctuations are considered as weak pressure or density fluctuations that propagate to the stationary regions of the same continuum where the effects of flow unsteadiness have completely decayed. The governing equations for the fluid flow are the unsteady compressible Navier–Stokes and energy equations; they are given as

$$\frac{\partial \rho}{\partial t} + \frac{\partial(\rho u_\alpha)}{\partial x_\alpha} = 0 \quad (1)$$

$$\frac{\partial(\rho u_\alpha)}{\partial t} + \frac{\partial(\rho u_\alpha u_\beta)}{\partial x_\beta} = -\frac{\partial p}{\partial x_\alpha} + \frac{\partial \tau_{\alpha\beta}}{\partial x_\beta} \quad (2)$$

$$\frac{\partial(\rho h)}{\partial t} + \frac{\partial(\rho h u_\alpha)}{\partial x_\alpha} = \left(\frac{\partial \rho}{\partial t} + u_\alpha \frac{\partial \rho}{\partial x_\alpha} \right) + \Phi + \frac{\partial}{\partial x_\alpha} \left(\kappa \frac{\partial T}{\partial x_\alpha} \right) \quad (3)$$

where u_α and x_α are the velocity component and position coordinate in the α direction, p is pressure, ρ is fluid density, and summation over repeated indices α and β is assumed. The viscous stress $\tau_{\alpha\beta}$ and the dissipation rate Φ are given by

$$\tau_{\alpha\beta} = 2\mu \left(S_{\alpha\beta} + \frac{1}{3} \delta_{\alpha\beta} S_{\chi\chi} \right), \quad \Phi = \tau_{\alpha\beta} S_{\alpha\beta}$$

$$S_{\alpha\beta} = \frac{1}{2} \left(\frac{\partial u_\alpha}{\partial x_\beta} + \frac{\partial u_\beta}{\partial x_\alpha} \right) \quad (4)$$

where Stokes hypothesis with zero bulk viscosity is invoked to deduce the viscous stresses, μ is the first coefficient of viscosity of the fluid, and κ is the fluid thermal conductivity. The viscosity μ and thermal conductivity κ are regarded as functions of temperature. Equations (1–4) are closed once the thermodynamic coupling of the internal energy, the pressure and the density is specified by the ideal gas equation of state, that is,

$$p = \rho RT \quad (5)$$

where $R = c_p - c_v$ is the gas constant and c_p and c_v are the specific heats at constant pressure and constant volume, respectively.

The conventional approach for aeroacoustics simulation proceeds by truncating the governing equations, or their linearized forms, in the spatial domain. The temporal evolutions are resolved by means of finite difference or finite volume techniques. On the other hand, if DNS is used to simulate aeroacoustics problems instead of the conventional methods, Eqs. (1–5) are solved directly. This way, it is possible to deduce and analyze the flowfield in detail. Because the acoustics quantities could be as small as $10^{-4} \sim 10^{-6}$ of the mean flow quantities, high-accuracy schemes are required if the sound field are to be resolved correctly with minimum numerical errors. This imposes a rather heavy penalty on the DNS scheme. In view of the credibility and accuracy of the DNS scheme, it is used in the present study as a benchmark to assess the proposed LBM scheme. The DNS solutions are obtained by solving Eqs. (1–5) using a sixth-order spatial scheme and a fourth-order Runge–Kutta time-marching scheme. Because the boundary conditions are associated with the aeroacoustics problems to be calculated, they will be discussed when the specific cases are analyzed. Details of the DNS scheme and its solutions of specific aeroacoustics problems are given elsewhere³³; therefore, they will not be repeated here.

III. One-Step LBM Aeroacoustics Simulation

To simulate aeroacoustics problems correctly using a one-step LBM approach, it is necessary to demonstrate that Eqs. (1–5) can be recovered properly. This requires the ideal gas equation of state with $\gamma = 1.4$ and μ to be recovered correctly from the LBM formulation. An attempt to accomplish this is carried out in the following sections.

Continuous BE

The basis of the LBM is the connection between the BE describing the kinetic theory of gases and the macroscopic equations of fluid flow. In kinetic theory, a simple dilute gas, such as air, is represented as a cloud of particles and is fully described by a continuous particle distribution function,³⁴ $f(x, \xi, t)$, which is the probability of finding a gas particle at location x moving with microscopic velocity ξ at time t . The tracking of f gives rise to a mesoscopic description of the fluid. This description is an intermediate step between the macroscopic continuum model and the microscopic description, which treats the fluid as an avalanche of discrete interacting gas molecules. For a dilute gas in which only binary collisions between particles occur, the evolution of the distribution function is governed by the continuous BE,

$$\frac{\partial f}{\partial t} + \xi \cdot \nabla f + F_{\text{ex}} \cdot \nabla_\xi f = Q(f, f)$$

$$= \int d^3\xi' \int d\Omega \sigma(\Omega) |\xi - \xi'| [f(\xi')f(\xi'_1) - f(\xi)f(\xi_1)] \quad (6)$$

The left-hand side of Eq. (6) describes the motions of streaming particles. The variable F_{ex} indicates external body force due to gravity or of electromagnetic origin. Because the rate of particle collision is not affected by the external body force, $F_{\text{ex}} = 0$ is assumed in the present formulation as a first attempt to solve Eq. (6). The operator Q accounts for the binary particle collision occurring within a differential collision cross section $\sigma(\Omega)$, which transforms the velocities from the (incoming) space $\{\xi, \xi_1\}$ to the (outgoing) space $\{\xi', \xi'_1\}$. For elastic collisions, the mass, momentum, and kinetic energy of the particles are conserved. Consequently, Q must possess exactly five collision invariants $\psi_s(\xi)$, $s = 0, 1, 2, 3, 4$, in the sense that

$$\int Q(f, f) \psi_s(\xi) d^3\xi = 0$$

The elementary collision invariants are $\psi_0 = 1$, $(\psi_1, \psi_2, \psi_3) = \xi$ and $\psi_4 = |\xi|^2$, which are proportional to mass, momentum, and kinetic energy of the fluid, respectively.

The nonlinear integro-differential equation (6) completely describes the spatiotemporal behavior of a dilute gas, but it is quite difficult to solve due to the complicated mathematical structure of Q for the closure problem.³⁴ Nevertheless, some measurable macroscopic averages of the flow can be defined from the velocity moments of the distribution function, for example, the zero- and first-order moments will give ρ and ρu , or

$$\rho = \int f d\xi \quad (7)$$

$$\rho u = \int \xi f d\xi \quad (8)$$

The definition of the fluid internal energy e needs further consideration of the molecular nature of the fluid. As will be indicated, realization of the diatomic nature of the fluid molecules is crucial to a successful recovery of the equation of state for a perfect gas, which is the key to a correct estimate of the first coefficient of viscosity and, hence, proper simulations of aeroacoustics problems.

A monoatomic gas model was commonly assumed in most previous LBM treatments. In this model, each gas particle supports only translational motion with only a D_T degree of freedom. This assumption does not appear to be appropriate for aeroacoustics computation because the fluid medium of interest is mostly air, which is mainly composed of diatomic nitrogen and oxygen gases. Generally, a polyatomic gas particle can undergo rotational motion with an additional D_R degree of freedom. This indicates that both translational and rotational kinetic energies of polyatomic gas particles should be taken into account in a proper definition of the macroscopic internal energy. The total number of degrees of freedom is $D_T + D_R = 5$ for diatomic gas such as air.³⁵ From the statistical mechanics point of view, the kinetic energy should be equally distributed by all degrees of freedom of gas particle motions. Following the arguments described in Appendix A, the macroscopic internal energy of the fluid can be defined by the second velocity moment as

$$\rho e + \frac{1}{2} \rho |u|^2 = \frac{D_T + D_R}{D_T} \int \frac{1}{2} f |\xi|^2 d\xi \quad (9)$$

Similarly, the fluid energy flux can be defined by the third velocity moment as

$$\left(\rho e + p + \frac{1}{2} \rho |u|^2 \right) u = \frac{D_T + D_R}{D_T} \int \frac{1}{2} f |\xi|^2 \xi d\xi \quad (10)$$

Integration of Eq. (9) suggests an explicit internal energy definition $e = (D_T + D_R)RT/2$ for diatomic gas. Actually, it can be shown that, with the definitions of macroscopic fluid variables described in Eqs. (7–10), the compressible Navier–Stokes equations and the perfect gas equation of state can be completely recovered from the BE and certain microscopic collision models through the Chapman–Enskog expansion (see Ref. 36).

Collision Model and the Chapman–Enskog Expansion

The collision operator Q contains all of the details of the binary particle interactions, but it is very difficult to evaluate due to the complicated structure of the integral. Simpler expressions for Q have been proposed. The idea behind that replacement is that the vast amount of details of the particle interactions is not likely to influence significantly the values of many experimentally measured macroscopic quantities.^{34,35} It is expected that the fine structure of $Q(f, f)$ can be replaced by a blurred image based on a simpler operator $J(f)$, which retains only the qualitative and average properties of the true operator. Furthermore, the H theorem shows that the average effect of collisions is to modify f by an amount proportional to the departure from the local Maxwellian–Boltzmann equilibrium distribution f^{eq} , which is expressed in D spatial dimensions as

$$f^{\text{eq}} = [\rho / (2\pi RT)^{D/2}] \exp(-|\xi - u|^2 / 2RT) \quad (11)$$

Therefore, the collision operator is approximated as $J(f) = -\omega(f - f^{\text{eq}})$. In case of a fixed collision interval, that is, $\omega = 1/\tau$, the well-known Bhatnagar–Gross–Krook³⁷ (BGK), or single-relaxation-time (SRT) model for monoatomic gas is recovered, and Eq. (6) is expressed as the Boltzmann–BGK kinetic model,

$$\frac{\partial f}{\partial t} + \xi \cdot \nabla_x f = -\frac{1}{\tau} (f - f^{\text{eq}}) \quad (12)$$

where τ is the time taken for a nonequilibrium f to approach f^{eq} .

The relaxation time τ is much smaller than the free movement time of the particle. It is the basic timescale in the BE. The disparity in the Boltzmann and macroscopic timescales indicates that all macroscopic quantities have converged to local equilibrium states at a very fast rate. The two disparate timescales in fact facilitate the derivation of the macroscopic compressible Navier–Stokes equations and their transport coefficients from the kinetic model of Eq. (12) by means of the Chapman–Enskog expansion (see Ref. 36). In essence, it is a standard multiscale expansion in which time and spatial dimensions are rescaled with the Knudsen number ε as a small expansion parameter, so that

$$\begin{aligned} t_1 &= \varepsilon t, & t_2 &= \varepsilon^2 t, & x_1 &= \varepsilon x \\ \frac{\partial}{\partial t} &= \varepsilon \frac{\partial}{\partial t_1} + \varepsilon^2 \frac{\partial}{\partial t_2}, & \frac{\partial}{\partial x} &= \varepsilon \frac{\partial}{\partial x_1} \end{aligned} \quad (13)$$

and the distribution function f is expanded as

$$f = f^{\text{eq}} + f^{\text{neq}} = f^{(0)} + \varepsilon f^{(1)} + \varepsilon^2 f^{(2)} + \mathcal{O}(\varepsilon^3) \quad (14)$$

The Knudsen number ε is the ratio of the mean free path between two successive particle collisions and the characteristic spatial scale of the fluid system. When $\varepsilon \sim \mathcal{O}(1)$ or larger, the gas in the system under consideration can no longer be considered as a fluid. When Eq. (14) is inserted into Eq. (12), terms with the same order of ε are collected, the resulting equation are multiplied with $\psi_s(\xi)$, and subsequent integration is performed over $d\xi^3$ in the velocity space, the following conservation laws are obtained:

$$\frac{\partial \rho}{\partial t} + \frac{\partial(\rho u_\alpha)}{\partial x_\alpha} = 0 \quad (15)$$

$$\begin{aligned} \frac{\partial(\rho u_\alpha)}{\partial t} + \frac{\partial(\rho u_\alpha u_\beta)}{\partial x_\beta} &= -\frac{\partial}{\partial x_\alpha} \left(\frac{2}{D_T + D_R} \rho e \right) \\ &+ \frac{\partial}{\partial x_\alpha} \left[\mu \left(\frac{\partial u_\beta}{\partial x_\alpha} + \frac{\partial u_\alpha}{\partial x_\beta} \right) \right] + \frac{\partial}{\partial x_\alpha} \left(\lambda \frac{\partial u_\gamma}{\partial x_\gamma} \right) \end{aligned} \quad (16)$$

$$\begin{aligned}
& \frac{\partial}{\partial t} \left(\rho e + \frac{1}{2} \rho u^2 \right) + \frac{\partial}{\partial x_\alpha} \left(\rho e + \frac{2\rho e}{D_T + D_R} + \frac{1}{2} \rho u^2 \right) \\
&= \frac{\partial}{\partial x_\alpha} \left(\kappa \frac{\partial e}{\partial x_\alpha} \right) + \frac{\partial}{\partial x_\alpha} \left[\mu u_\beta \left(\frac{\partial u_\beta}{\partial x_\alpha} + \frac{\partial u_\alpha}{\partial x_\beta} \right) \right] \\
&+ \frac{\partial}{\partial x_\alpha} \left(\lambda \frac{\partial u_\gamma}{\partial x_\gamma} u_\alpha \right) \quad (17)
\end{aligned}$$

It is clear that Eqs. (15–17) are the macroscopic conservation equations needed for a flow governed by the compressible Navier–Stokes equations with the first coefficient of viscosity, the second coefficient of viscosity, and the thermal diffusivity defined as

$$\mu = (\gamma - 1) \rho e \tau \quad (18)$$

$$\lambda = -(\gamma - 1)^2 \rho e \tau \quad (19)$$

$$\kappa' = \gamma(\gamma - 1) \rho e \tau \quad (20)$$

In Eqs. (16) and (17), the terms associated with the second viscosity, that is, $\lambda(\partial u_\gamma / \partial x_\gamma)$, are generally small compared to the other terms in practical flows³⁸; therefore, they could be neglected in the following analysis. The relation between κ and κ' in the present formulation is $\kappa = \kappa' c_v / Pr$. Comparing these expressions with the macroscopic energy conservation Eq. (3) leads to $\mu c_p = \kappa$ and consequently a Prandtl number of unity in the present formulation. A different Prandtl number could be assigned by scaling the value $(D_T + D_R) / D_T$ in Eqs. (9) and (10), but it was not attempted in the present paper.

The fluid properties are all dependent on τ , which is a function of T because the relaxation phenomenon depends on T . Therefore, the temperature behavior of the fluid properties is, to a great extent, governed by the relation between τ and T . In the following section, the ideal gas equation is derived first, and this is followed by a derivation of μ based on a SRT model for J . The need for another τ model besides the SRT is shown.

Equation of State and the Specific Heat Ratio

If the pressure and the ratio of specific heats are defined as $p = 2\rho e / (D_T + D_R)$ and $\gamma = (D_T + D_R + 2) / (D_T + D_R)$, respectively, then the ideal gas equation of state follows:

$$p = (\gamma - 1) \rho e = \rho RT$$

which is identical to Eq. (5). Since $D_T + D_R = 5$, $\gamma = 1.4$ and the ideal gas equation of state are recovered correctly using the Chapman–Enskog expansion to facilitate the derivation of the unsteady compressible Navier–Stokes equations.

In most numerical simulations of aerodynamics and aeroacoustics based on macroscopic conservation laws, the value of μ is usually estimated from the Sutherland law. The law of viscosity based on Sutherland's model of intermolecular force potential shows that the dependence of μ on T takes the following form:

$$\mu = \frac{5}{16\sqrt{\pi}} \frac{1}{\sigma_m^2} \frac{\sqrt{M_n k_B T}}{1 + S_0/T} \approx \left(\frac{T}{T_{\text{ref}}} \right)^{\frac{3}{2}} \frac{T_{\text{ref}} / T + S_0 / T}{1 + S_0 / T} \quad (21)$$

where T_{ref} is a reference temperature and S_0 is the Sutherland constant, equal to 111, 107, and 139 K for air, nitrogen, and oxygen, respectively (see Ref. 39). The error associated with this approximation is within 2–4% over a temperature range of 210–1900 K. If the LBM scheme were to be credible, it should recover μ correctly; otherwise, the Reynolds number effect of unsteady flows would be incorrectly captured.

According to Eq. (12), a SRT model is tacitly assumed for τ . In other words, a rigid-sphere collision model is assumed, and the kinetic model admits a relaxation time for particle velocity expressed as³⁸

$$\tau \approx \frac{5}{4} \bar{\tau} = \frac{5}{4} \frac{\bar{\lambda}}{|\bar{\xi}|} = \frac{5}{4} \frac{1}{\sqrt{2\pi n \sigma_m^2 |\bar{\xi}|}} = \frac{5}{4\sqrt{2}} \left(1 / \pi n \sigma_m^2 \sqrt{\frac{8k_B T}{\pi M_n}} \right) \quad (22)$$

where $\bar{\lambda}$ is the average mean free path, $\bar{\tau}$ is the time interval of particle collision and $|\bar{\xi}| = \sqrt{(8k_B T / \pi M_n)}$ is the magnitude of the mean particle velocity. This gives a relation between τ and T and allows the determination of μ from Eq. (18). Combining Eqs. (5) and (18) gives $\mu = (\gamma - 1) \rho e \tau = p \tau = \rho RT \tau$. Simple manipulation then shows that

$$\mu \approx (5/16\sqrt{\pi}) (1/\sigma_m^2) \sqrt{M_n k_B T} \quad (23)$$

Equation (23) clearly indicates that μ has a different T dependence compared to Eq. (21), the Sutherland law. This means that real gas effects on μ cannot be modeled properly from the microscopic SRT model. If μ were to reflect the correct temperature dependence as indicated in Eq. (21), another model for τ has to be proposed.

IV. Recovery of the Correct First Coefficient of Viscosity

The phenomenon of fluid viscosity could be attributed to momentum transfer between gas particles before and after collisions. The distributions of momenta of the particles depend on the momentum of each particle when they are far separated, as well as the interactions of intermolecular potentials when two particles are in close encounter. The intermolecular potential represents the contributions of intermolecular attraction and repulsion to the potential function. According to Ferziger and Kaper,³⁹ from the kinetic theory point of view, SRT is equivalent to the adoption of a rigid-sphere model in which the short-range force potential behaves as if a Dirac-delta function with finite repulsion at the separation when two rigid particles are in contact (particle separation $r_m = \sigma_m$). The model yields an exaggerated potential change at $r_m \approx \sigma_m$ and predicts poorly the temperature dependence of the macroscopic fluid properties. Sutherland (see Ferziger and Kaper³⁹) then suggests to include a weak but rapidly decaying repulsive potential, $\sim (\sigma_m / r_m)^v$ (v being the index of repulsion), in the interaction and successfully provides a more realistic description of the dependence of μ on temperature, such as given by Eq. (21). The effects of this weak potential might be more pronounced in the relaxation of a diatomic gas due to its more complicated molecular structure. The question then is how to account for this weak potential effect. As a first attempt, it is proposed to include the relaxation times associated with both the intermolecular potential and the weak repulsive potential in the estimate of τ for the BGK collision model invoked in Eq. (12).

It is assumed that τ in Eq. (12) can be replaced by an effective relaxation time τ_{eff} and that this could be determined from a combination of the relaxation times associated with the intermolecular potential τ_1 and the weak repulsive potential τ_2 . The relation between τ_{eff} , τ_1 , and τ_2 together with separate expressions for τ_1 and τ_2 have to be determined. According to Ferziger and Kaper,³⁹ τ_1 could be estimated from the rigid-sphere model. Therefore, τ_1 is given by Eq. (22). It can be rewritten as

$$\tau_1 \approx (5/4) \bar{\tau} \propto 1 / \sqrt{T} \quad (24)$$

The determination of τ_2 is much more complicated because it depends on the particle velocity as well as on the physical nature of the gas under consideration. It could be argued that because the weak potential is a long-range potential, τ_2 could be postulated to be proportional to the average approach velocity of the particles, that is,

$$\tau_2 \propto |\bar{\xi}| \propto T^{\frac{1}{2}} \quad (25)$$

The dependence of τ_2 on T is, therefore, known; however, the exact relation has yet to be determined. Its determination will become clear after a thorough comparison of the derived μ has been made with the Sutherland law.

With the functional form known for τ_1 and τ_2 , the next step is to determine τ_{eff} so that the LBM scheme would yield a correct μ in addition to being able to recover the ideal gas equation of state. How to relate τ_{eff} to τ_1 and τ_2 can be gleaned from an examination of the derivation of μ as shown in Eq. (23) and Sutherland law. It is obvious that an SRT based on the rigid-sphere model would give an incorrect representation for μ . The discrepancy is in the T dependence. If the correct dependence on T were to be recovered, the

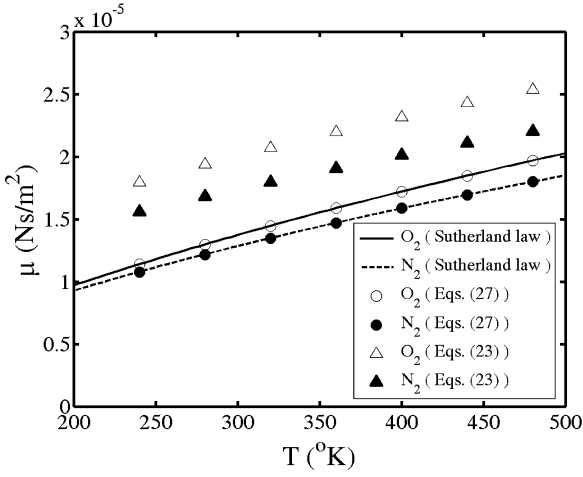


Fig. 1 Variations of first coefficient of viscosity with temperature and its comparison with Sutherland law.

right-hand side of Eq. (23) should be multiplied by a factor proportional to $1/(1 + S_0/T)$. Because τ_1/τ_2 is proportional to $1/T$, this suggests representing τ_{eff} by $\tau_{\text{eff}} = \tau_1/(1 + \tau_1/\tau_2)$. Consequently, the simplified collision operator J can be expressed as

$$J(f) = -(1/\tau_{\text{eff}})(f - f^{\text{eq}}) = -1/[\tau_1 \tau_2 / (\tau_1 + \tau_2)](f - f^{\text{eq}}) \quad (26)$$

The procedure used to derive Eq. (23) can be repeated using Eq. (26) for $J(f)$. The result is

$$\mu = \rho RT \tau_{\text{eff}} = \rho RT \left/ \left(\frac{1}{\tau_1} + \frac{1}{\tau_2} \right) \right. \approx \frac{5}{16\sqrt{\pi}} \frac{1}{\sigma_m^2} \frac{\sqrt{M_n k_B T}}{1 + \tau_1/\tau_2} \quad (27)$$

A comparison of Eq. (27) with Eq. (21) clearly shows that τ_1/τ_2 should be related to S_0/T by the simple expression $\tau_1/\tau_2 = S_0/T$. This is the relation for the determination of τ_2 . Thus derived, the LBM scheme will yield a μ that has the proper dependence on T .

A comparison of the Sutherland law with the derived viscosity relations can now be made. Figure 1 shows the variations of μ for two common diatomic gases, nitrogen and oxygen, as calculated using Eqs. (23) and (27) and the Sutherland law. It is evident that the SRT model overpredicts the values of μ for a wide range of temperature with errors ranging from 28% at high temperature to 70% at low temperature. On the other hand, the two-relaxation-time (τ_1 and τ_2) model yields results that are in excellent agreement with those given by the Sutherland law. Theoretical analysis⁴⁰ shows that the acoustic properties of a fluid can be fully and accurately resolved by a multiple-relaxation-time (MRT) model in which τ [in Eq. (12)] for each velocity moment can be adjusted separately. However, adoption of an MRT model would require complicated programming to adjust τ for each velocity moment, thus, giving rise to higher computational cost. As will be seen in later comparison with DNS and theoretical results, the present model will also yield fully and accurately the acoustic properties of the fluid with much less complication in programming for the same problem.

V. Numerical Scheme

Instead of tracking the evolutions of the primitive variables in the flow solutions in conventional numerical flow simulations, the method of LBM solves only the evolution of f as prescribed in Eq. (12). This equation is first discretized in a velocity space using a finite set of velocity vectors $\{\xi_i\}$ in the context of the conservation laws²⁷ such that

$$\frac{\partial f_i}{\partial t} = -\xi_i \cdot \nabla_x f_i - \frac{1}{\tau_{\text{eff}}} (f_i - f_i^{\text{eq}}) \quad (28)$$

where $f_i(x, t) = f(x, \xi_i, t)$ is the distribution function associated with the α th discrete velocity ξ_i and f_i^{eq} is the corresponding equi-

librium distribution function in the discrete velocity space. The continuous local Maxwellian f^{eq} may be rewritten up to the third order of the velocity after a Taylor expansion in u and can be expressed in the discrete velocity space as

$$f^{\text{eq}} = \rho A_i \left\{ 1 + \frac{\xi \cdot u}{\theta} + \frac{(\xi \cdot u)^2}{2\theta^2} - \frac{u^2}{2\theta} - \frac{(\xi \cdot u)u^2}{2\theta^2} + \frac{(\xi \cdot u)^3}{6\theta^3} + \mathcal{O}\left(\frac{u^4}{\theta^2}\right) \right\} \quad (29)$$

where $u = (u, v)$ and $\theta = RT$. The weighting factors A_i are dependent on the lattice model selected to represent the discrete velocity space. They are evaluated from the constraints of local macroscopic variables [Eqs. (7–10)] in the lattice with N discrete velocity sets, as

$$\begin{aligned} \rho &= \sum_{i=1}^N f_i^{\text{eq}}, & \rho e + \frac{1}{2} \rho |u|^2 &= \frac{D_T + D_R}{D_T} \sum_{i=1}^N \frac{1}{2} f_i^{\text{eq}} |\xi_{\alpha}|^2 \\ \rho u &= \sum_{i=1}^N \xi_i f_i^{\text{eq}} \\ \left(\rho e + p + \frac{1}{2} \rho |u|^2 \right) u &= \frac{D_T + D_R}{D_T} \sum_{i=1}^N \frac{1}{2} f_i^{\text{eq}} |\xi_i|^2 \xi_i \end{aligned} \quad (30)$$

For the two-dimensional diatomic gas flow considered in the present study, two discrete velocity sets are attempted for the lattice, namely, a D2Q9 model and a D2Q13 model. For the D2Q9 model (Fig. 2a),

$$\begin{aligned} \xi_0 &= 0 \\ \xi_i &= c(\cos[\pi(i-1)/4], \sin[\pi(i-1)/4]), & i &= 1, 3, 5, 7 \\ \xi_i &= \sqrt{2}c(\cos[\pi(i-1)/4], \sin[\pi(i-1)/4]), & i &= 2, 4, 6, 8 \\ A_0 &= 1 + 2\gamma\theta^2 - 3\theta \\ A_1 &= A_3 = A_5 = A_7 = -\gamma\theta^2 + \theta \\ A_2 &= A_4 = A_6 = A_8 = (\gamma/2)\theta^2 - \frac{1}{4}\theta \end{aligned}$$

For the D2Q13 model (Fig. 2b),

$$\begin{aligned} \xi_0 &= 0 \\ \xi_i &= c(\cos[\pi(i-1)/4], \sin[\pi(i-1)/4]), & i &= 1, 3, 5, 7 \\ \xi_i &= \sqrt{2}c(\cos[\pi(i-1)/4], \sin[\pi(i-1)/4]), & i &= 2, 4, 6, 8 \\ \xi_i &= 2c(\cos[\pi(i-1)/2], \sin[\pi(i-1)/2]), & i &= 9, 10, 11, 12 \end{aligned}$$

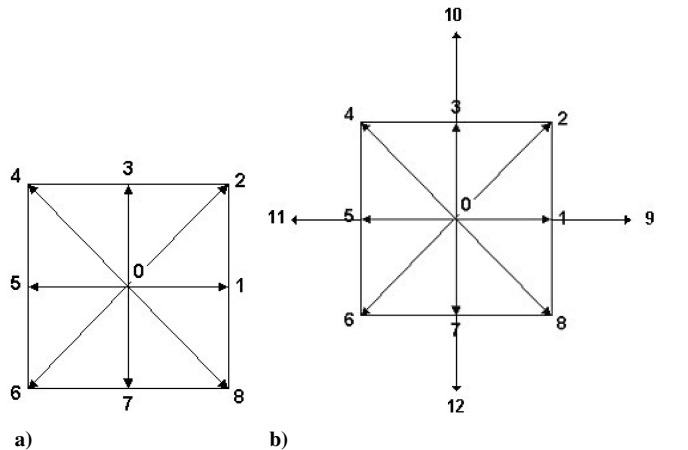


Fig. 2 Lattice velocity models: a) D2Q9 and b) D2Q13.

$$\begin{aligned}
A_0 &= 1 - (5/2)\theta + [-3/2 + 2\gamma]\theta^2 \\
A_1 &= A_3 = A_5 = A_7 = (2/3)\theta + (1 - \gamma)\theta^2 \\
A_2 &= A_4 = A_6 = A_8 = [-3/4 + (1/2)\gamma]\theta^2 \\
A_9 &= A_{10} = A_{11} = A_{12} = -(1/24)\theta + (1/8)\theta^2
\end{aligned}$$

It is evident from later comparisons that the D2Q13 model yields more accurate results; hence, it is preferred.

The collision process represented by J on the right-hand side of Eq. (28) is evaluated locally at every time step, whereas the streaming process represented by the convective derivatives of f_i are evaluated by a sixth-order finite difference scheme.¹¹ The time-dependent term on the left-hand side of Eq. (28) is calculated by time marching using a second-order Runge–Kutta scheme. No numerical filter is used for the following cases in the present study. These treatments have minimal effects on the numerical viscosity for small quantity disturbances, and so a one-step numerical simulation of the BE could lead to realistic prediction of aeroacoustics problems where the results are essentially identical to those derived from similar DNS solutions and theoretical results.

VI. Results and Discussion

Many practical aeroacoustics simulations aim to predict sound radiation created by unsteady flows and their interactions with solid boundaries. Correct simulation of wave propagation is an important measure of the success of a numerical model for aeroacoustics simulation. With all viscous terms neglected, Eqs. (1) and (2) reduce to the Euler equation that supports three modes of waves, namely, acoustic, vorticity, and entropy waves. The acoustic waves are isotropic, nondispersive, nondissipative, and propagate with the speed of sound $c = \sqrt{(\gamma RT)}$. The vorticity and entropy waves are nondispersive, nondissipative, and propagate in the same direction of the mean flow with the same velocity of the flow. Propagations of the three types of waves are selected for the validation of the present LBM scheme. The accuracy of the LBM aeroacoustics simulation is assessed by comparing the LBM calculations with the DNS results obtained by using convectional finite difference method³³ to solve the two-dimensional fully compressible unsteady Navier–Stokes equations. A measure of the difference between the LBM and DNS results of a macroscopic variable b is expressed in terms of the L_p integral norm, that is,

$$\|L_p(b)\| = \left[\frac{1}{M} \sum_{b=1}^M |b_{\text{LBM},j} - b_{\text{DNS},j}|^p \right]^{1/p} \quad (31)$$

for any integer p and its maximum

$$\|L_\infty(b)\| = \max_j |b_{\text{LBM},j} - b_{\text{DNS},j}| \quad (32)$$

Three example test cases are carried out to validate the proposed LBM. These are 1) the propagation of a plane pressure pulse in stationary fluid in a tube, 2) the propagation of a circular pulse in stationary fluid, and 3) simulations of an acoustic, an entropy, and a vortex pulse convected with subsonic uniform mean flow velocity u_0 . In the first two cases, the nondimensional parameters for the length, time, density, velocity, pressure, and temperature are specified as L_0 , L_0/c_0 , ρ_0 , c_0 , ρc_0^2 , and T_0 , and the Reynolds number is defined by $Re = \rho_0 L_0 c_0 / \mu$. For the LBM, the pressure is implied in the kinetic equation and can be deduced from the state equation, $p = (\gamma - 1)\rho e$. The normalized internal energy and sound speed are given by $e = T/[\gamma(\gamma - 1)]$ and $c = \sqrt{T}$. In the third case, the nondimensional parameters for time, density, velocity, pressure, and temperature are L_0/u_0 , ρ_0 , u_0 , ρu_0^2 , and T_0 , respectively, and $M = u_0/c_0$ is the Mach number. The LBM and DNS solutions are compared in all three cases. In case 3, analytical solutions are also available¹⁰; these, too, will be shown for comparisons with the LBM and DNS solutions. All physical quantities in the following discussion are dimensionless, except where specified.

Case 1: Propagation of a Plane Pressure Pulse

This one-dimensional problem aims to validate the accuracy and robustness of the proposed LBM and, at the same time, to assess the efficiency of the proposed lattice models. The distribution function $f_i(x, t) = f(x, \xi_i, t)$ is developing with the collision function and the streaming function of Eq. (28). The initial fluid state is defined as a small plane pressure fluctuation in the center of a tube, such that

$$\rho = \rho_\infty \quad (33a)$$

$$u = 0 \quad (33b)$$

$$v = 0 \quad (33c)$$

$$p = p_\infty + \varepsilon \exp(-\ell_n 2 \times x^2 / 0.08^2) \quad (33d)$$

where mean field density and pressure are given by $\rho_\infty = 1$ and $p_\infty = 1/\gamma$, the pulse amplitude ε is set to 4×10^{-6} , 16×10^{-6} , and 100×10^{-6} , respectively, and $Re = 5000$ is specified in this case. The computational domain size of the tube is $-5 \leq x \leq 5$ by $0 \leq y \leq 2$. A uniform grid of size 0.02×0.02 is adopted. Slip boundary conditions are applied on the upper and lower tube surfaces in the DNS calculation. The stability criterion³¹ of the collision term requires that the time step should be $\Delta t < \tau/2$; therefore, $\Delta t = 0.0001$ is chosen for the present LBM computations. Two buffer zones are specified in the DNS calculation to simulate a true nonreflecting inlet and outlet boundary condition.³³ For all LBM calculations, the gradient of the distribution function on all boundaries are set to zero. When all disturbances are far away from the numerical boundaries, these conditions can ensure that there is essentially no error contribution coming from the boundary treatment.

In case 1, the initial conditions Eq. (33) essentially combine one acoustic wave and one entropy wave. These two waves overlap the density fluctuations with each other only for the initial state. After the acoustic wave leaves the center area, the density fluctuations created by the entropy wave would appear in the center. Figure 3 shows the fluctuations along the centerline of the tube at $t = 1.0$ and 3.0 for the case $\varepsilon = 100 \times 10^{-6}$. The LBM and DNS simulations show a slight difference in the density at the center when the acoustic pulse propagates toward computational boundaries. (Further calculations carried out after the manuscript had been accepted showed that the slight difference at the center was due to an error in setting the initial value of f at that point.) However, the density distribution in the central region is essentially the same. The two positive density fluctuation peaks are leaving the center with a propagation speed $c = 1$, and the amplitude of this density fluctuation is $\hat{p} = 4 \times 10^{-5}$ ($t = 3.0$). At the same corresponding positions, there are two pressure fluctuation peaks with a value of $\hat{p} = 4 \times 10^{-5}$. Actually these two waves are the exact acoustic waves because the transmission speed is the physical sound speed and the amplitudes follow the acoustic relation $\hat{p} = c^2 \hat{\rho}$. These results show that the proposed LBM can replicate the correct acoustic waves and the calculated macroscopic quantities are developing correctly, just as the DNS solution indicates.

This is evident from a comparison of the calculated $\|L_p(p)\|$ (pressure). Figure 4 shows the time-dependent difference in the behavior of $\|L_1(p)\|$, $\|L_2(p)\|$, and $\|L_\infty(p)\|$ ($\varepsilon = 4 \times 10^{-6}$). Both lattice D2Q9 and D2Q13 solutions are reported. The differences between the LBM and DNS solutions using the D2Q13 lattice are much smaller than those using the D2Q9 lattice. For example, consider the $\|L_2(p)\|$ value, the difference obtained for the D2Q13 lattice is about 10^{-11} , whereas the corresponding value for the D2Q9 lattice is close to 10^{-9} . This shows that the D2Q13 lattice could effect an improvement in $\|L_p(p)\|$ of two orders of magnitude when only four more discrete velocities are specified. In view of this, only the D2Q13 lattice model results are presented in the following discussion.

The pulse amplitude effect on the difference $\|L_2(p)\|$ is compared in Fig. 5. The criterion of a Taylor expansion on a Maxwellian distribution requires that the flow speed u to be much smaller than the particle speed ξ , and the error of this expansion would occur in the term of $\mathcal{O}(u^4/\theta^2)$. When the pulse amplitude is smaller, the disturbance u is also smaller. This would lead to a smaller error term $\mathcal{O}(u^4/\theta^2)$. Therefore, $\|L_2(p)\|$ would be smaller for $\varepsilon = 4 \times 10^{-6}$

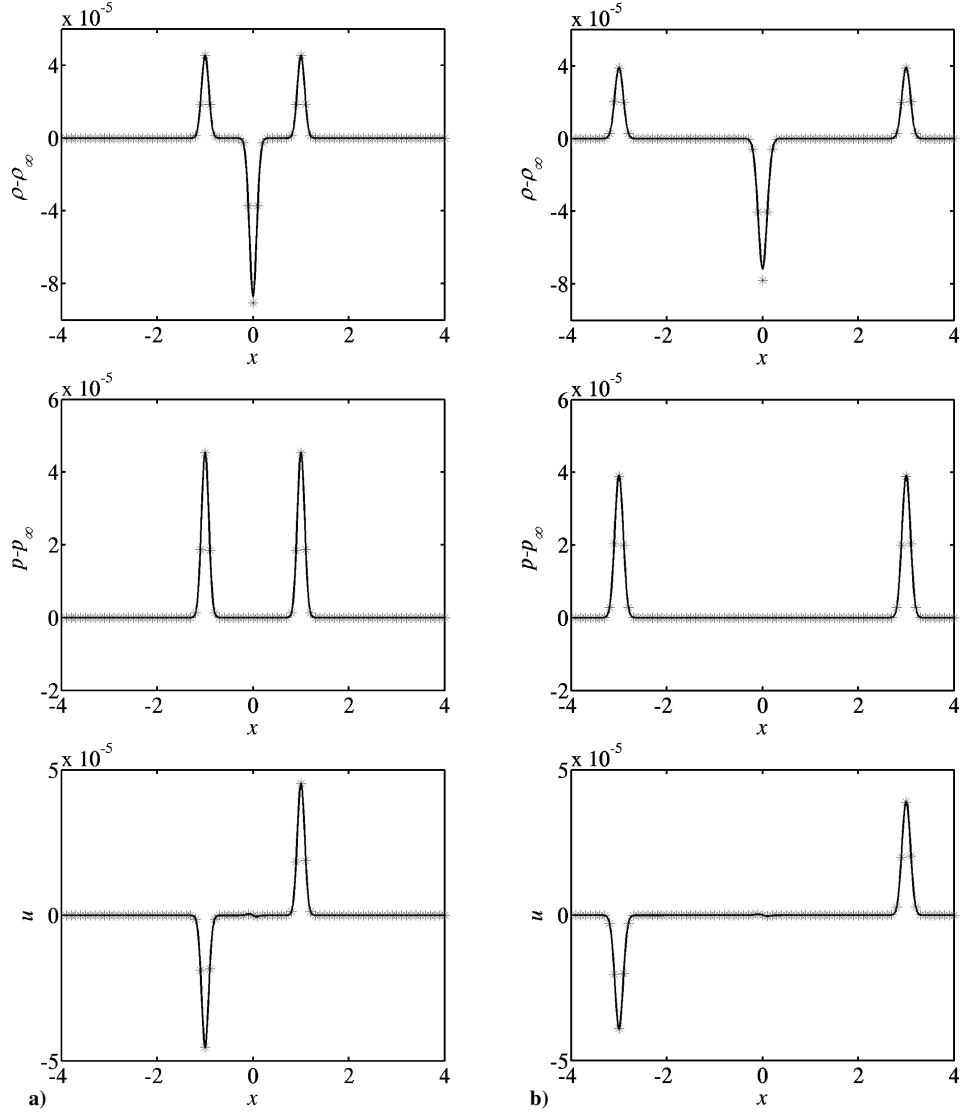


Fig. 3 Density, pressure, and velocity u fluctuations along the x axis at a) $t=1.0$ and b) $t=3.0$ for $\varepsilon=100 \times 10^{-6}$: *, LBM (D2Q13) and —, DNS.

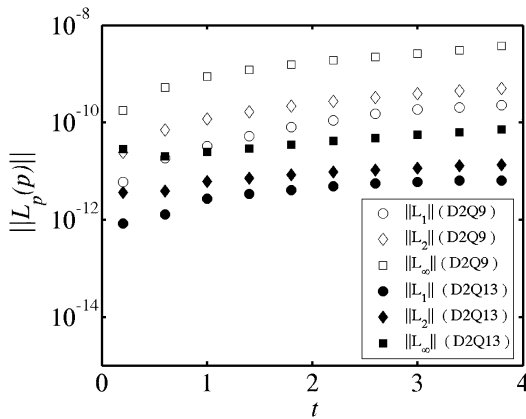


Fig. 4 Time history of the difference $\|L_p(p)\|$.

than for $\varepsilon = 16 \times 10^{-6}$ and 100×10^{-6} . This result is clearly demonstrated in Fig. 5, which shows that the performance of the LBM is better with smaller fluctuations than those large fluctuations.

Case 2: Propagation of a Circular Pulse

If an initial circular pulse is imparted to a uniform fluid, the fluctuations thus created would propagate equally in all directions. This means that, at any time, the pulse would remain circular in shape. However, the lattice velocity model restricts the particles to

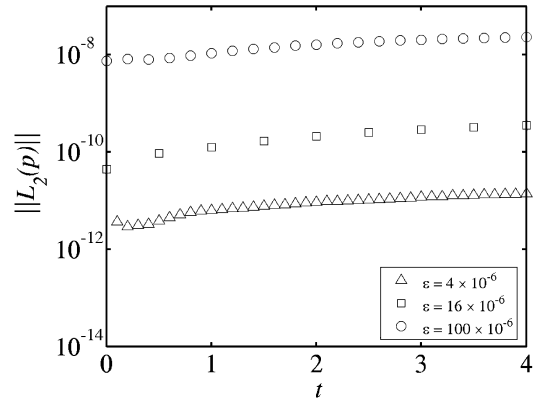


Fig. 5 Time history of the difference $\|L_2(p)\|$ with D2Q13.

move in certain discrete directions, such as $0, \pm\pi/4, \pm\pi/2$, and π (Fig. 2). To test the ability of the LBM with a D2Q13 lattice model to replicate the symmetry property of the circular pulse, it is used to simulate a circular initial pressure pulse in a uniform fluid. The distribution is defined as

$$\rho = \rho_\infty \quad (34a)$$

$$u = 0 \quad (34b)$$

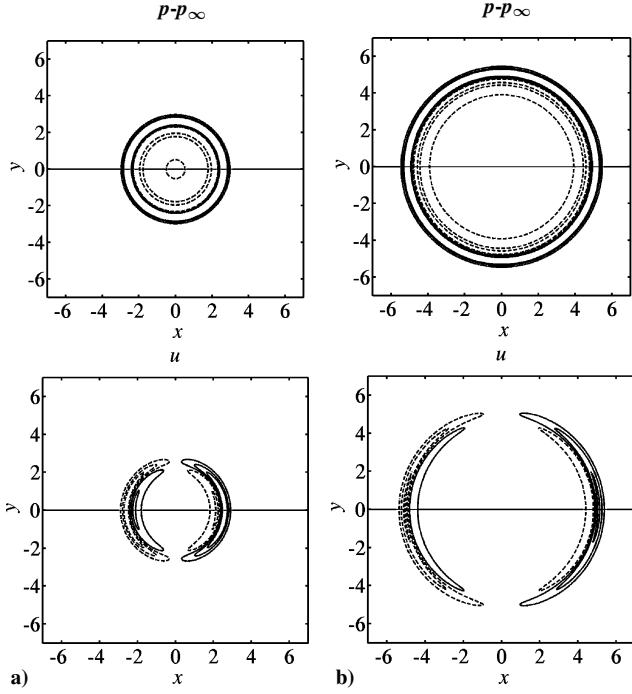


Fig. 6 Pressure and velocity fluctuations at a) $t = 2.5$ and b) $t = 5.0$: —, positive levels and - - -, negative levels.

$$v = 0 \quad (34c)$$

$$p = p_\infty + \varepsilon \exp[-\ln 2 \times (x^2 + y^2)/0.2^2] \quad (34d)$$

where $\rho_\infty = 1$, $p_\infty = 1/\gamma$, $\varepsilon = 16 \times 10^{-6}$, and $Re = 5000$. The computational domain is 20×20 , and the grid size is 0.05×0.05 . Both LBM and DNS are used to simulate this problem.

The contours of the pressure and u fluctuations are shown in Fig. 6. The upper-half of the computation domain is the LBM solution and the lower-half the DNS solution at the same time. For pressure fluctuations, six contours are equally distributed between -0.4×10^{-6} and 0.4×10^{-6} ; for velocity fluctuations, six contours are equally distributed between -1×10^{-6} and 1×10^{-6} . It is clear that the contours of the LBM solution have no discernible difference with those of the DNS result. This is despite that the LBM solution is derived from a velocity lattice model D2Q13, where particle velocities are specified for discrete directions only. This shows that the LBM simulation is just as valid as the DNS result.

Case 3: Simulations of Acoustic, Entropy, and Vortex Pulses

The acoustic, entropy, and vorticity pulses are basic fluctuations in aeroacoustics problems. In this case, the pulses are developing in a uniform mean flow. Basically, only the acoustic pulse is propagating with the sound speed; the entropy pulse and the vortex pulse would move with the mean flow. The initial conditions are defined as

$$\rho = \rho_\infty + \varepsilon_1 \exp\{-\ln 2 \times [(x+1)^2 + y^2]/0.2^2\} + \varepsilon_2 \exp\{-\ln 2 \times [(x-1)^2 + y^2]/0.4^2\} \quad (35a)$$

$$u = u_\infty + \varepsilon_3 y \exp\{-\ln 2 \times [(x-1)^2 + y^2]/0.4^2\} \quad (35b)$$

$$v = v_\infty + \varepsilon_3 (x-1) \exp\{-\ln 2 \times [(x-1)^2 + y^2]/0.4^2\} \quad (35c)$$

$$p = p_\infty + (1/M^2)\varepsilon_1 \exp\{-\ln 2 \times [(x+1)^2 + y^2]/0.2^2\} \quad (35d)$$

where $M = 0.2$ and $\varepsilon_1 = 0.0001$, $\varepsilon_2 = 0.001$, and $\varepsilon_3 = 0.001$. The mean field has density, speed, and pressure given by $\rho_\infty = 1$, $u_\infty = 1$ and $v_\infty = 0$, and $p_\infty = 1/(\gamma M^2)$, and $Re = 1000$. These pulse models follow the definitions of Tam (see Ref. 10). The acoustic pulse is initialized at the point $x = -1$, $y = 0$. The entropy pulse and the vorticity pulse are initialized at $x = 1$, $y = 0$. The computational domain

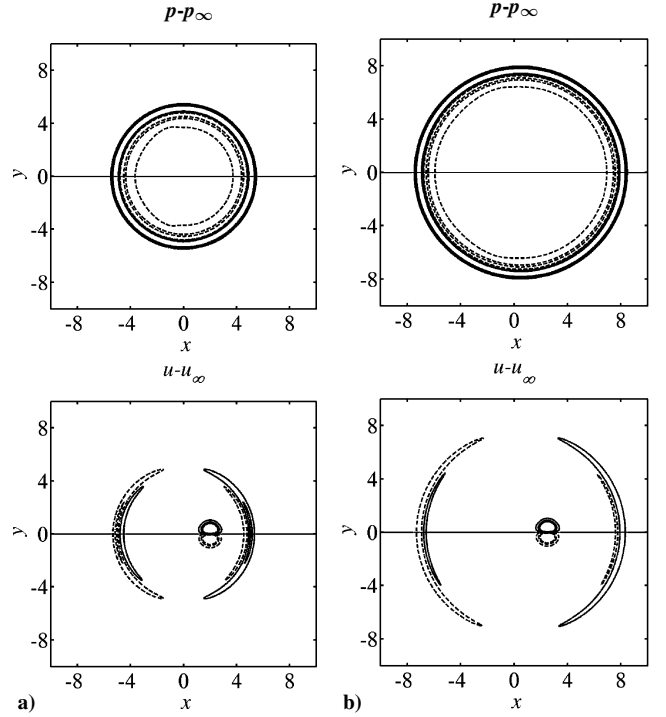


Fig. 7 Pressure and velocity fluctuations at a) $t = 1.0$ and b) $t = 1.5$: —, positive levels and - - -, negative levels.

is $-10 \leq x \leq 10$ by $-10 \leq y \leq 10$, and the grid size is 0.05×0.05 . For this problem with a relatively large mean flow, the mean flow effect could become critical because the symmetry lattice coefficients are based on the assumption that the flow speed is much smaller than the particle speed. An improvement to the proposed LBM model is given in Appendix B to address this problem.

The pressure and the u velocity fluctuation contours are shown in Fig. 7 at $t = 1.0$ and 1.5 . Both LBM and DNS results are shown together. The initial acoustic pulse causes disturbances. Because the mean flow speed is defined as 1.0, the center of the pulse has moved to $x = 0$, $y = 0$ at $t = 1.0$, and to $x = 0.5$, $y = 0$ at $t = 1.5$. The acoustic pressure fluctuation is propagating with $c = 1/M = 5$ and exhibit circles of radii equal to 5 and 7.5 at the same moment. The u velocity fluctuation is symmetric about the x axis. For the vorticity pulse, the center of the vortex would move to $x = 2$, $y = 0$ at $t = 1.0$ and to $x = 2.5$, $y = 0$ at $t = 1.5$. In Fig. 7, the upper-half of the domain is the LBM solution; the lower-half the domain is the DNS solution. For pressure fluctuations, six contours are equally distributed between -5×10^{-5} and 5×10^{-5} ; for velocity fluctuations, six contours are equally distributed between -5×10^{-5} and 5×10^{-5} . The distribution of the u velocity fluctuation from this pulse would give the same absolute fluctuations that propagate along the negative x axis. The pressure and u velocity fluctuations are in Fig. 8. The LBM and DNS simulations are essentially identical, and they agree well with the analytical inviscid solutions.¹⁰

The same case with $Re = 100$ is also calculated to investigate the effect of viscosity on the LBM simulation. The pressure and velocity fluctuations at $t = 1.0$ are compared in Fig. 9, where the distributions along $-6 \leq x \leq 0$ are shown. The asterisks represent the LBM solution, whereas the DNS result is given by the dotted line. The solid line shows the analytical inviscid solution. Again, LBM and DNS give essentially the same solution and are close to the inviscid result. There is a discernible viscous effect on the acoustic pulse, which is essentially a disturbance generated from the viscous effect on the entropy pulse. The $\|L_p\|$ differences for pressure and u velocity fluctuations are given in Table 1.

There are two macroscopic velocity scales in case 3, namely, the mean flow velocity and the fluctuation propagation velocity. To assess the correctness of the LBM in resolving small-fluctuation propagation in a mean flow, it is worthwhile to study the spreading

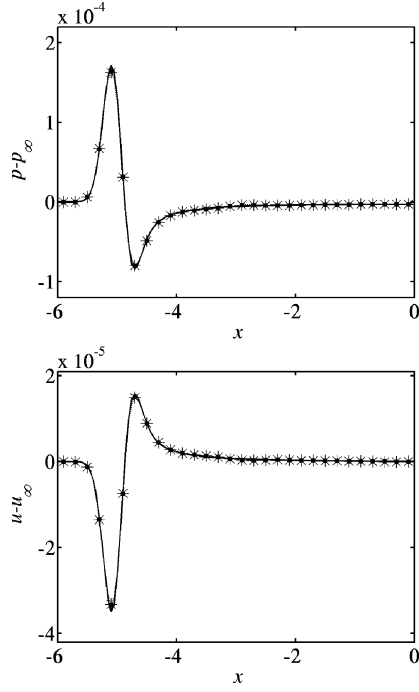


Fig. 8 Pressure and velocity fluctuation distributions along x axis at $t = 1.0$ and $Re = 1000$: —, analytical inviscid solution; *, LBM solution; and ●, DNS solution.

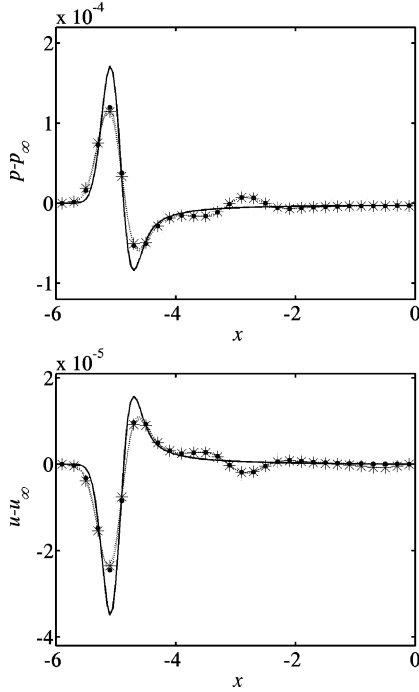


Fig. 9 Pressure and u velocity fluctuation distributions along x axis at $t = 1.0$ and $Re = 100$: —, analytical inviscid solution; *, LBM solution; and ●, DNS solution.

of the acoustic pulse. Figure 10 shows the decay of acoustic pulse peak in LBM and DNS solutions at $Re = 100$ and 1000 . The analytical result is also shown. For an acoustic pulse spreading in two dimensions, the local intensity of the wave I should be proportional to $1/r$ due to conservation of total energy $e = I \cdot 2\pi r$, where r is the radial distance. In the absence of viscosity, the intensity bears a relationship with instantaneous pressure peak amplitude A as $I \propto A^2$. Therefore, the analytical result should be a straight line in Fig. 10 with slope equal to $-\frac{1}{2}$. For $Re = 1000$, the amplitudes are very close to the inviscid solution, indicating the acoustic propagation is

Table 1 L_p difference and the effect of Reynolds number^a

Trial	L_1	L_2	L_∞
$L_p = \left(\frac{1}{N} \sum_{-6 < x < 0} (\hat{p} - p_r)^p \right)^{1/p}$			
LBM ($Re = 1000$)	$8.8339e-007$	$1.8589e-006$	$8.9069e-006$
DNS ($Re = 1000$)	$8.0505e-007$	$1.6447e-006$	$7.5991e-006$
LBM ($Re = 100$)	$6.8489e-006$	$1.3173e-005$	$5.8618e-005$
DNS ($Re = 100$)	$6.4574e-006$	$1.2113e-005$	$5.1829e-005$
$L_p = \left(\frac{1}{N} \sum_{-6 < x < 0} (\hat{u} - u_r)^p \right)^{1/p}$			
LBM ($Re = 1000$)	$1.8577e-007$	$3.7268e-007$	$1.7917e-006$
DNS ($Re = 1000$)	$1.6058e-007$	$3.2878e-007$	$1.5348e-006$
LBM ($Re = 100$)	$1.4394e-006$	$2.6432e-006$	$1.1803e-005$
DNS ($Re = 100$)	$1.2827e-006$	$2.4207e-006$	$1.0477e-005$

^aHere, $\hat{p} = p - p_\infty$, $\hat{u} = u - u_\infty$ and p_r, u_r are the analytical solutions.

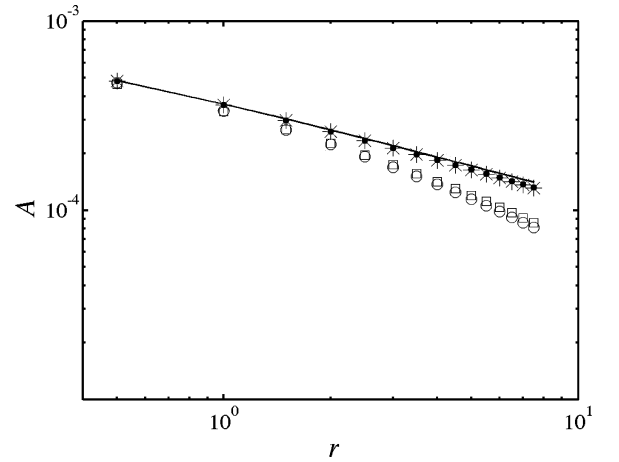


Fig. 10 Variation of pressure peak amplitude with the radius of the acoustic pulse travels: —, analytical inviscid solution; *, LBM ($Re = 1000$); ●, DNS ($Re = 1000$); ○, LBM ($Re = 100$); and □, DNS ($Re = 100$).

correctly captured with a viscous formulation in the DNS and LBM calculations at this Reynolds number. For $Re = 100$, the LBM and DNS solutions are essentially identical. The difference in peak amplitude is only 6% after the pulse has propagated a distance equal to 19 times the initial pulse width ($r = 7.5$). It can be observed that viscosity has a significant effect and gives rise to a difference of about 20% between the $Re = 100$ and $Re = 1000$ cases at the same distance.

With the comparison of the performance of the LBM with the DNS in the simulations of one-step aeroacoustics problems made, a word about the programming and computational requirements of the two different methods is in order. In terms of programming, the LBM is much simpler. The LBM code consists of 420 lines compared to 1350 lines required for the DNS code. As for the computational time required, the CPU time for calculating 1000 time steps using a 100×100 grid differ for the three cases tested. For the plane pressure pulse case (one dimensional), the LBM is 25% more efficient than the DNS; for the circular pulse case (two dimensional), the DNS is about 20% more efficient; whereas for the three pulses case, the DNS is about 30% more efficient. These comparisons are made with the D2Q13 velocity lattice model. If the D2Q9 model is used instead, the LBM is more efficient by a margin ranging from 15 to 50% for the three cases tested. However, the $\|L_p(b)\|$ accuracy suffers by two orders of magnitude (Fig. 4).

VII. Conclusions

An LBM scheme has been formulated for one-step aeroacoustics simulations. In the formulation, the definition of fluid internal

energy has been modified to include both the translational and rotational degrees of freedom of the particles. The collision model is modified to take into account the relaxation times associated with the intermolecular potential and the weak repulsive potential. With these modifications, the ideal gas equation of state with $\gamma = 1.4$ is recovered exactly and the first coefficient of viscosity of the gas has the correct temperature dependence. Consequently, the set of unsteady compressible Navier–Stokes equations is fully recovered for aeroacoustics simulations. Two lattice (D2Q9 and D2Q13) models were used to carry out calculations for diatomic gases. A sixth-order finite difference scheme is used to evaluate the streaming term, and a second-order time-marching technique is used to calculate the time-dependent term in the BE, whereas the collision term is evaluated locally. Three test cases were used to validate the LBM. They are the one-dimensional acoustic pulse propagation, the circular acoustic pulse propagation, and the propagation of acoustic, vorticity, and entropy pulses in a uniform mean flow. The accuracy of the method is established by comparing the calculations with analytical solutions and with DNS results obtained with a sixth-order spatial scheme and a fourth-order Runge–Kutta time-marching scheme. All comparisons show that the LBM aeroacoustics simulation possesses the same accuracy as DNS solutions for CAA and is a simpler numerical method.

It is especially convenient to use LBM to simulate aeroacoustics problems numerically. First, the inherent linearity of the governing Boltzmann equation and the numerical efficiency of the LBM allow the intrinsic features of parallelism²³ to be exploited. Second, the LBM offers new opportunities for kinetic-type nonreflecting boundary conditions. These two difficulties are common in most CAA but could be overcome with further developments of LBM. Finally, the results of test cases 1–3 reflect that the present two-relaxation-time LBM scheme correctly captures the physical sound speed for $0.2 \leq M \leq 1.0$. This contrasts with the extremely narrow Mach number range ($M \rightarrow 0$) for conventional SRT LBM scheme. For the sake of completeness, it is important to investigate whether the present LBM scheme can capture the high sound speed in the limit of $M < 0.2$. This issue will be discussed in a companion paper.

Appendix A: Definition of Internal Energy

The internal energy e is defined by the following relation:

$$\rho e + \frac{1}{2}\rho|u|^2 = \frac{D_T + D_R}{D_T} \int \frac{1}{2} f |\xi|^2 d\xi \quad (\text{A1})$$

In general, the particle distribution function f can be decomposed into an equilibrium part and a nonequilibrium part, that is, $f = f^{\text{eq}} + f^{\text{neq}}$. The nonequilibrium f^{neq} is required to satisfied the nullity requirement for moments of different velocity orders, that is,

$$\int f^{\text{neq}} d\xi = \int f^{\text{neq}} \xi d\xi = \int f^{\text{neq}} \xi^2 d\xi = 0 \quad (\text{A2})$$

Therefore, with use of Eq. (11) for f^{eq} , Eq. (A1) can be expressed as

$$\begin{aligned} \rho e + \frac{1}{2}\rho|u|^2 &= \frac{D_T + D_R}{D_T} \int \frac{1}{2} f^{\text{eq}} |\xi|^2 d\xi \\ &= \frac{D_T + D_R}{D_T} \int \frac{1}{2} \frac{\rho}{(2\pi RT)^{D/2}} \exp\left(-\frac{|\xi - u|^2}{2RT}\right) |\xi|^2 d\xi \end{aligned} \quad (\text{A3})$$

The total number of degrees of freedom for diatomic gas motions is always $D_T + D_R = 5$ (where $D_T = 3$ and $D_R = 2$). Therefore, the right-hand side of Eq. (A3) is a function of temperature alone. The sole temperature effect on e is realized in the redistribution of the particle momentum due to particle collision and should be independent of the mean flow velocity carrying the particles.³¹ Therefore, e should be the same irrespective of whether $u = 0$. Integration of

Eq. (A3) in three-dimensional simulations ($D = 3$) leads to

$$\begin{aligned} e &= \frac{D_T + D_R}{3} \int_0^\infty 4\pi r^2 \frac{1}{2} \frac{1}{(2\pi RT)^{\frac{3}{2}}} \exp\left(-\frac{|r|^2}{2RT}\right) |r|^2 dr \\ &= \frac{D_T + D_R}{3} \left(\frac{3}{2} RT\right) = \frac{D_T + D_R}{2} RT \end{aligned} \quad (\text{A4})$$

where $r = \xi - u$.

In a two-dimensional simulation, only two planar translational motions are allowed, thus giving $D_T = 2$. If similar arguments for the temperature dependence in the three-dimensional case is applied, then, with $r = \xi - u$ in two dimensions,

$$\begin{aligned} e &= \frac{D_T + D_R}{2} \int_0^\infty 2\pi r \frac{1}{2} \frac{\rho}{(2\pi RT)} \exp\left(-\frac{|r|^2}{2RT}\right) |r|^2 dr \\ &= \frac{D_T + D_R}{2} RT \end{aligned} \quad (\text{A5})$$

Evidently, the definition of e in the present LBM holds for both two- and three-dimensional flows. Note that the integration results of Eqs. (A3) and (A5) perfectly match the classical equipartition theorem of the kinetic theory of gases, which states that, for a polyatomic gas, each degree of freedom equally contributes $RT/2$ to the total amount of internal energy.

Appendix B: LBM with Mean Flow

The Taylor expansion of the local Maxwellian, Eq. (11), in the discrete velocity space is given by Eq. (29). The assumption of symmetry coefficients of the lattice requires that the velocity u to be much smaller than the particle speed. When the effective flow speed is large, the truncation error in this expansion would increase. For the present problem, the macroscopic flow velocity is about the same as the mean flow velocity \bar{u} . This means that the fluctuation velocity $u - \bar{u}$ is much smaller than the particle speed. When the local Maxwellian is rewritten with this interpretation, Eq. (11) can be expressed as

$$f^{\text{eq}} = \frac{\rho}{(2\pi RT)^{D/2}} \exp\left(-\frac{|(\xi - \bar{u}) - (u - \bar{u})|^2}{2RT}\right) \quad (\text{B1})$$

where $u - \bar{u}$ is the relative flow velocity based on the mean flow and it is much smaller than the particle speed. When the lattice velocity speed is defined based on the total part of $\xi - \bar{u}$, the coefficient of the lattice still satisfies the symmetry assumption. Therefore, the Taylor expansion of f^{eq} [Eq. (29)] can be expressed as

$$\begin{aligned} f^{\text{eq}} &= \rho A_i \left\{ 1 + \frac{(\xi - \bar{u}) \cdot (u - \bar{u})}{\theta} + \frac{[(\xi - \bar{u}) \cdot (u - \bar{u})]^2}{2\theta^2} - \frac{(u - \bar{u})^2}{2\theta} \right. \\ &\quad \left. - \frac{[(\xi - \bar{u}) \cdot (u - \bar{u})](u - \bar{u})^2}{2\theta^2} + \frac{[(\xi - \bar{u}) \cdot (u - \bar{u})]^3}{6\theta^3} \right\} \end{aligned} \quad (\text{B2})$$

This expansion can be used with the earlier symmetry lattice to discretize the velocity $u - \bar{u}$. The discretized velocities in the lattice are defined as $\xi_T = (0, 0), (1, 0), (0, 1), \dots$; therefore, the real particle speed becomes $\xi = \bar{u} + \xi_T$. The original Boltzmann equation in the discretized space can then be written as

$$\frac{\partial f_i}{\partial t} = -(\xi_{Ti} + \bar{u}) \cdot \nabla f_i - \frac{1}{\tau} (f_i - f_i^{\text{eq}}) \quad (\text{B3})$$

It follows that the kinetic equations will become

$$\rho = \int f d\xi_T \quad (\text{B4})$$

$$\rho(u - \bar{u}) = \int \xi_T f d\xi_T \quad (\text{B5})$$

$$\rho e + \frac{1}{2}\rho|u - \bar{u}|^2 = \frac{D_T + D_R}{D_T} \int \frac{1}{2} f |\xi_T|^2 d\xi_T \quad (\text{B6})$$

$$\left(\rho e + p + \frac{1}{2}\rho|(u - \bar{u})|^2\right)(u - \bar{u}) = \frac{D_T + D_R}{D_T} \int \frac{1}{2} f |\xi_T|^2 \xi_T d\xi_T \quad (\text{B7})$$

When $\bar{u} = (0, 0)$, Eqs. (B4–B7) reduce to Eqs. (7–10). If there is an effective macroscopic mean flow, only the relative velocity $u - \bar{u}$ is considered in the Taylor expansion and the kinetic equations. Again, the relative velocity is much smaller than the particle speed, and so the symmetry coefficients can be used but the evolution equation is given by Eq. (B3). This method is proven useful in case 3.

Acknowledgment

Support given by the Research Grants Council of the Government of the Hong Kong Special Administrative Region under Grants PolyU5174/02E, PolyU5303/03E, and PolyU1/02C is gratefully acknowledged.

References

- ¹Tam, C. K. W., "Computational Aeroacoustics: Issues and Methods," *AIAA Journal*, Vol. 33, No. 10, 1995, pp. 1788–1796.
- ²Singer, B. A., Lockard, D. P., and Lilley, G. M., "Hybrid Acoustic Predictions," *Computer and Mathematics with Applications*, Vol. 46, No. 4, 2003, pp. 647–669.
- ³Lighthill, M. J., "On Sound Generated Aerodynamically: I. General Theory," *Proceedings of the Royal Society of London, Series A: Mathematical and Physical Sciences*, Vol. 211, No. 1107, 1952, pp. 564–587.
- ⁴Ffowcs Williams, J. E., and Hawkins, D. L., "Sound Generation by Turbulence and Surfaces in Arbitrary Motion," *Philosophical Transactions of Royal Society of London, Series A: Mathematical and Physical Sciences*, Vol. 264, No. 1151, 1969, pp. 321–342.
- ⁵Bogey, C., Baily, C., and Juvé, D., "Computation of Flow Noise Using Source Terms in Linearized Euler's Equation," *AIAA Journal*, Vol. 40, No. 2, 2002, pp. 235–243.
- ⁶Hardin, J. C., and Pope, D. S., "An Acoustic/Viscous Splitting Technique for Computational Aeroacoustics," *Theoretical and Computational Fluid Dynamics*, Vol. 6, No. 5–6, 1994, pp. 323–340.
- ⁷Shen, W. Z., and Sorensen, J. N., "Aeroacoustic Modeling of Low-Speed Flows," *Theoretical and Computational Fluid Dynamics*, Vol. 13, No. 4, 1999, pp. 271–289.
- ⁸Colonius, T., "Modeling Artificial Boundary Conditions for Compressible Flow," *Annual Review of Fluid Mechanics*, Vol. 36, 2004, pp. 315–345.
- ⁹Wells, V. L., and Renaut, R. A., "Computing Aerodynamically Generated Noise," *Annual Review of Fluid Mechanics*, Vol. 29, 1997, pp. 161–199.
- ¹⁰Tam, C. K. W., and Webb, J. C., "Dispersion-Relation-Preserving Finite Difference Schemes for Computational Aeroacoustics," *Journal of Computational Physics*, Vol. 107, No. 2, 1993, pp. 262–281.
- ¹¹Lele, S. K., "Compact Finite Schemes with Spectral-Like Resolution," *Journal of Computational Physics*, Vol. 103, No. 1, 1992, pp. 16–42.
- ¹²Holberg, O., "Computational Aspects of the Choice of Operator and Sampling Interval for Numerical Differentiation in Large-Scale Simulation of Wave Phenomena," *Geophysical Prospecting*, Vol. 35, No. 6, 1987, pp. 629–655.
- ¹³Casper, J., and Meadows, K. R., "Using High-Order Accurate Essentially Nonoscillatory Schemes for Aeroacoustic Application," *AIAA Journal*, Vol. 34, No. 2, 1996, pp. 244–250.
- ¹⁴Kim, C., Roe, P. L., and Thomas, J. P., "Accurate Schemes for Advection and Aeroacoustics," AIAA Paper 97-2091, June–July 1997.
- ¹⁵Visbal, M. R., and Gaitonde, D. V., "Very High-Order Spatially Implicit Schemes for Computational Acoustics on Curvilinear Meshes," *Journal of Computational Acoustics*, Vol. 9, No. 4, 2001, pp. 1259–1286.
- ¹⁶Tam, C. K. W., "Advances in Numerical Boundary Conditions for Computational Aeroacoustics," *Journal of Computational Acoustics*, Vol. 6, No. 4, 1998, pp. 377–402.
- ¹⁷Harris, S., *An Introduction to the Theory of the Boltzmann Equation*, Dover, New York, 1999, Chaps. 1–4.
- ¹⁸Wolf-Gladrow, D. A., *Lattice-Gas Cellular Automata and Lattice Boltzmann Models. An Introduction*, Springer, New York, 2000, Chap. 5.
- ¹⁹Hirschfelder, J. O., Curtiss, C. F., and Bird, R. B., *Molecular Theory of Gases and Liquids*, Wiley, New York, 1964, p. 15.
- ²⁰Yu, D., Mei, R., Luo, L.-S., and Shyy, W., "Viscous Flow Computations with the Method of Lattice Boltzmann Equation," *Progress in Aerospace Sciences*, Vol. 39, 2003, pp. 329–367.
- ²¹Chen, S., and Doolen, G. D., "Lattice Boltzmann Method for Fluid Flows," *Annual Review of Fluid Mechanics*, Vol. 30, 1998, pp. 329–364.
- ²²Succi, S., *The Lattice Boltzmann Equation for Fluid Dynamics and Beyond*, Oxford Univ. Press, New York, 2001.
- ²³Chen, H., Chen, S., and Matthaeus, W. H., "Recovery of the Navier–Stokes Equations Using a Lattice-Gas Boltzmann Method," *Physical Review A: General Physics*, Vol. 45, 1992, pp. 5339–5342.
- ²⁴Qian, Y. H., d'Humières, D., and Lallemand, P., "Lattice BGK Models for Navier–Stokes Equation," *Europhysics Letters*, Vol. 17, No. 6, 1992, pp. 479–484.
- ²⁵Frisch, U., Hasslacher, B., and Pomeau, Y., "Lattice-Gas Automata for the Navier–Stokes Equation," *Physical Review Letters*, Vol. 56, No. 14, 1986, pp. 1505–1508.
- ²⁶Frisch, U., d'Humières, D., Hasslacher, B., Lallemand, P., Pomeau, Y., Rivet, J.-P., and Pomeau, Y., "Lattice Gas Hydrodynamics in Two and Three Dimensions," *Complex Systems*, Vol. 1, 1987, pp. 649–707.
- ²⁷He, X., and Luo, L.-S., "Theory of the Lattice Boltzmann Method: From the Boltzmann Equation to Lattice Boltzmann Equation," *Physical Review E: Statistical, Nonlinear, and Soft Matter Physics*, Vol. 56, No. 6, 1997, pp. 6811–6817.
- ²⁸Lallemand, P., and Luo, L.-S., "Theory of the Lattice Boltzmann Method: Dispersion, Dissipation, Isotropy, Galilean Invariance, and Stability," *Physical Review E: Statistical, Nonlinear, and Soft Matter Physics*, Vol. 61, No. 6, 2000, pp. 6546–6562.
- ²⁹Sun, C., "Lattice-Boltzmann Models for High Speed Flow," *Physical Review E: Statistical, Nonlinear, and Soft Matter Physics*, Vol. 58, No. 6, 1998, pp. 7283–7287.
- ³⁰Palmer, B. J., and Rector, D. R., "Lattice Boltzmann Algorithm for Simulating Thermal Flow in Compressible Fluids," *Journal of Computational Physics*, Vol. 161, No. 1, 2000, pp. 1–20.
- ³¹Tsukahara, M., Kataoka, T., Takada, N., Kang, H.-K., and Kurita, M., "Simulations of Compressible Flows by Using the Lattice Boltzmann and the Finite Difference Lattice Boltzmann Methods," *Computational Fluid Dynamics Journal*, Vol. 11, No. 1, 2002, pp. 486–493.
- ³²Kang, H.-K., Ro, K.-D., Tsukahara, M., and Lee, Y.-H., "Numerical Prediction of Acoustic Sounds Occurring by the Flow Around a Circular Cylinder," *KSME International Journal*, Vol. 17, No. 8, 2003, pp. 1219–1225.
- ³³Leung, R. C. K., Li, X. M., and So, R. M. C., "A Comparative Study of Non-Reflecting Condition for One-Step Numerical Simulation of Duct Aero-Acoustics," *AIAA Journal* (to be published).
- ³⁴Cercignani, C., *Theory and Application of the Boltzmann Equation*, Scottish Academic Press, Edinburgh, 1975.
- ³⁵Woods, L. C., *An Introduction to Kinetic Theory of Gases and Magnetoplasmas*, Oxford Univ. Press, New York, 1993, pp. 52–55.
- ³⁶Chapman, S., and Cowling, T. G., *The Mathematical Theory of Non-Uniform Gases*, Cambridge Univ. Press, Cambridge, England, U.K., 1970.
- ³⁷Bhatnagar, P., Gross, E. P., and Krook, M. K., "A Model for Collision Processes in Gases, I. Small Amplitude Processes in Charged and Neutral One-Component Systems," *Physical Review*, Vol. 94, No. 3, 1954, pp. 515–525.
- ³⁸White, F. M., *Viscous Fluid Flow*, McGraw–Hill, New York, 1991, pp. 27–29.
- ³⁹Ferziger, J. H., and Kaper, H. G., *Mathematical Theory of Transport Processes in Gases*, North-Holland, Amsterdam, 1975.
- ⁴⁰Lallemand, P., and Luo, L. S., "Theory of the Lattice Boltzmann Method: Acoustic and Thermal Properties in Two and Three Dimensions," *Physical Review E: Statistical, Nonlinear, and Soft Matter Physics*, Vol. 68, 2003, 036706.

D. Gaitonde
Associate Editor